Article

Accurate Structures and Rotational Constants of Steroid Hormones at DFT Cost: Androsterone, Testosterone, Estrone, *β*-Estradiol, and Estriol

Published as part of The Journal of Physical Chemistry A virtual special issue "Massimo Olivucci Festschrift".

Lina Uribe, Silvia Di Grande, Luigi Crisci, Federico Lazzari, Marco Mendolicchio, and Vincenzo Barone*

Cite This: *J. Phys. Chem. A* 2024, 128, 2629−2642

Read Online

ACCESS | Metrics & More | Article Recommendations | Supporting Information

ABSTRACT: A comprehensive analysis of the structural, conformational, and spectroscopic properties in the gas phase has been performed for five prototypical steroid hormones, namely, androsterone, testosterone, estrone, *β*-estradiol, and estriol. The revDSD-PBEP86 double-hybrid functional in conjunction with the D3BJ empirical dispersion and a suitable triple-ζ basis set provides accurate conformational energies and equilibrium molecular structures, with the latter being further improved by proper account of core−valence correlation. Average deviations within 0.1% between computed and experimental ground state rotational constants are reached when adding to those equilibrium values vibrational corrections obtained at the cost of standard harmonic frequencies thanks to the use of a new computational tool. Together with the intrinsic interest of the studied hormones, the accuracy of the results obtained at DFT cost for molecules containing about 50 atoms paves the way toward the accurate investigations of other flexible bricks of life.
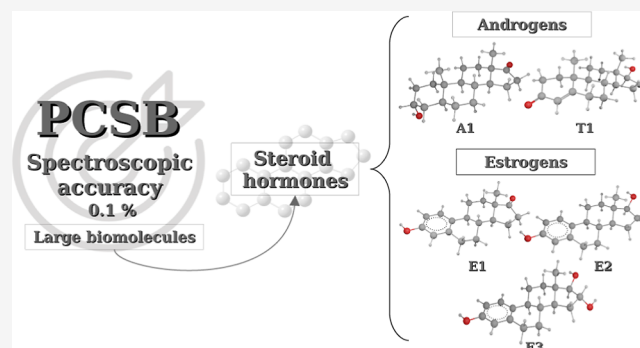
1. INTRODUCTION

The primary outcomes of microwave (MW) spectra are very accurate rotational constants, which are inversely proportional to moments of inertia and, consequently, depend on atomic masses and geometrical parameters.[1] Since the inception of MW spectroscopy in 1934 by Cleeton and Williams[2] and its increased success after 1945, systematic studies have been performed for gases and liquids with high vapor pressures. Only quite recently has it become possible to study solid substances with low vapor pressures and thermally fragile systems, including several molecular bricks of life.[3,4] This progress has been possible thanks to the combination of Fourier transform microwave (FTMW) spectroscopy with supersonic jets and laser ablation (LA),[4] leading to development of laser ablation molecular beam FTMW (LA-MB-FTMW)[5,6] and laser ablation chirped-pulse FTMW (LA-CP-FTMW).[7] Replacement of the LA by a heatable reservoir is also possible and is employed in the COMPACT (Compact-Passage-Acquired Coherence Technique) CP-FTMW spectrometer.[8] In any case, the assignment and interpretation of experimental MW spectra are not straightforward and are strongly aided by accurate quantum chemical (QC) computations,[9,10] with average relative errors below 0.1% (i.e., 1 MHz for a rotational constant of 1000 MHz) being required for unbiased analysis.[11]

The development of effective and robust computational strategies for the study of large flexible molecules faces two main difficulties: (i) the unsupervised sampling of the potential energy surface (PES) to determine the most stable low-energy structures (e.g., conformers or rotamers)[12] and (ii) the computation of accurate structures and spectroscopic parameters for the species obtained in step (i).[11,13,14] In the present paper, we will be mainly concerned with step (ii), which involves the calculation of very accurate equilibrium geometries and the inclusion of vibrational and, possibly, electronic contributions.[14] Several QC strategies have been developed to obtain accurate equilibrium structures for molecules of increasing dimensions, including different flavors of wave function composite schemes (CSs),[15−18] the semi-experimental (SE) approach[19−25] and the template molecule (TM)[26,27] or linear regression (LR)[27] models, together with their combination (TM-LR).[28−30] The best CSs rooted in the coupled cluster (CC) ansatz[31] provide structural parameters with an accuracy better than 1 mÅ for
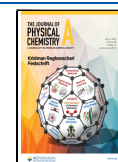
bond lengths and 0.1° for angles,[11,16,32] but they are very computationally demanding and cannot be applied to molecules containing about 50 atoms, which are the targets of the present study. The combination of experimental ground state rotational constants and QC vibrational corrections provides the SE equilibrium rotational constants. Then, a least-squares fitting of these quantities for a sufficient number of isotopologues produces the corresponding SE equilibrium structure (r^{SE}). While the SE approach gives access to high-quality geometrical parameters,[21,27,29,30,33] the large number of isotopologues needed for a robust fitting is available only for relatively small molecules. For larger molecules, the development of the TM and LR strategies has allowed us to overcome the lack of sufficient experimental data and/or the prohibitive cost of accurate QC computations. Both approaches are based on the assumption that if enough data are available (either experimental or computational) for a subset of molecules, it is possible to refine larger systems by looking at their fragments (templating molecules) for which accurate data are accessible. The corrections derived from those fragments are then applied to the computed geometrical parameters of the target molecule to obtain the final high-quality equilibrium structure. In the TM strategy, the correction is the difference between the accurate geometrical parameters of a set of templating molecules containing suitable fragments of the target molecule and the corresponding parameters computed at the same level employed to study the (larger) target. On the other hand, the LR correction is obtained from a LR fit of the geometrical parameters of a large database of high-quality reference molecules, without any supervised assignment of molecular fragments.

The recent Pisa composite scheme[34,35] employs density functional theory (DFT)[36] and second-order Møller−Plesset perturbation (MP2) theory[37] to draw closer to the so-called spectroscopy accuracy avoiding the expensive CC method, without the use of any empirical parameter (in addition to those possibly present in the underlying DFT model). The workflow requires the combination of geometry optimizations performed at three different computational levels, namely, rev-DSD-PBEP86-D3BJ/cc-pVTZ-F12 (rDSD/3F12) together with frozen core (*fc*) and all-electron (*ae*) MP2/cc-pwCVTZ (MP2/wC3). The idea behind this approach is that the same core−valence (CV) contribution employed in several wave function CSs[38−41] can be added also to rev-DSD-PBEP86-D3BJ/cc-pVTZ-F12 geometries. The main drawbacks of the approach are related to the quite large basis set employed and the need to perform three different geometry optimizations. In order to deal with the first issue, the 3F12 basis set has been replaced by its smaller 3F12⁻ counterpart,[14] whereas the second issue is faced by replacing the MP2 step by a one-parameter bond correction.[42] The combination of rev-DSD-PBEP86-D3BJ functional and 3F12⁻ basis set will be referred to in the following simply as rDSD. In this connection, it is worth mentioning that, while the D4 model for empirical dispersion[43] might deliver marginally better results for energies,[44] D3BJ and D4 contributions to geometrical parameters are virtually indistinguishable, and, above all, analytical second derivatives are available only for the D3BJ version.[45]

Both variants of the model provide accurate equilibrium geometries (from which rotational constants) to which vibrational corrections need to be added. Since the vibrational corrections are much smaller (less than 1%) than equilibrium rotational constants, the cheaper B3LYP global

hybrid functional[46−48] augmented by D3BJ empirical dispersion[49,50] in conjunction with the 6-31+G* basis set[51−53] provides sufficiently accurate results.[34,42,54,55] This combination of the method and basis set will be referred to in the following simply as B3. Unfortunately, even at this level, the computation of the leading anharmonic contribution to vibrational corrections becomes cumbersome for molecules containing about 50 atoms, which are the targets of the present study. We have therefore developed a new engine employing analytical gradients that provides accurate results at the same cost as the evaluation of harmonic frequencies.

Thanks to all of these developments, it should be, in principle, possible to obtain equilibrium structures and ground state rotational constants of unprecedented accuracy for large molecules. The new tool has been validated by a systematic investigation of several steroid hormones (androsterone, testosterone, estrone, and *β*-estradiol), whose experimental MW spectra have been recorded in the last six years.[56−59] Such hormones, belonging to androgen and estrogen families, have a wide biological activity in the human body, are biosynthesized from cholesterol, and have a common semirigid backbone with different substituents.[60] We also analyzed estriol (another estrogen), whose structure and spectroscopic parameters have not yet been reported.

2. METHODS

2.1. Conformational Energies. The studied hormones involve only a limited number of soft degrees of freedom, so the powerful techniques developed for the conformational search of flexible molecules[61,62] are not needed, and systematic relaxed scans are sufficient. Furthermore, several studies have shown that accurate conformational energies can be obtained at the rDSD level without resorting to more sophisticated (and costly) composite wave function methods.[54,63−68] The same computational approach delivers accurate dipole moments,[69] whose components along the principal inertia axes determine the intensities of rotational transitions.[70]

The structures of the low-energy minima of androsterone, testosterone, estrone, and *β*-estradiol reported in previous studies[56−59,71] were used as starting points for full geometry optimizations at the rDSD level. On the other hand, the starting structures for estriol were obtained from those of *β*-estradiol by enforcing staggered conformations of its additional OH moiety.

As is well-known, conformational relaxation can take place under the experimental conditions whenever the energy barriers ruling the interconversion are sufficiently low, with an upper limit of $2k_BT$ ($\approx$400 cm^{-1} at 298 K) being usually employed for discriminating in rotational spectroscopy of flexible biomolecule building blocks.[72−74] With the aim of unravelling fast conformational relaxations, we always performed relaxed torsional scans to obtain preliminary information on low-energy interconversion paths. Next, after the precise location of the transition states (TSs) by full geometry optimizations, their nature was checked by computing and diagonalizing the corresponding Hessian matrices.

2.2. Accurate Structures and Rotational Constants. Several studies have shown that remarkably accurate geometries can be obtained resorting to the CCSD(T)-F12b ansatz[75] in conjunction with the cc-pVDZ-F12[76] (hereafter 2F12) basis set.[77] Then, a fortuitous, but very general, error compensation between overestimation (lack of post-MP2 contributions) and underestimation (limitation of the basis set) leads to very accurate results when the conventional MP2 model[37] is

employed in conjunction with the cc-pwCVTZ[78] (wC3) basis set to evaluate the contribution of CV correlation[79]

$$\Delta r^{CV} = r(ae - MP2/wC3) - r(fc - MP2/wC3) \quad (1)$$

As a consequence, the following estimates of equilibrium geometrical parameters (r^{PCS2}) are obtained

$$r^{PCS2} = r(CCSD(T) - F12b/2F12) + \Delta r^{CV} \quad (2)$$

Unfortunately, this approach becomes too expensive for molecules containing more than 10−15 atoms. Therefore, an accurate reduced-cost estimate of equilibrium geometries (referred to as PCS3D) has been recently introduced,[34] in which the Δr^{CV} contribution is retained, but the coupled cluster model is replaced by a cheaper DFT approach (in particular, the rev-DSD-PBEP86-D3BJ double-hybrid functional[44,49,50] in conjunction with the 3F12 basis set[76]). The resulting geometrical parameters are

$$r^{PCS3D} = r(DFT) + \Delta r^{CV} \quad (3)$$

As already mentioned in the Introduction, the computational cost can be reduced with negligible accuracy loss by replacing the 3F12 basis set by its 3F12$^-$ counterpart, in which the d function on first-row atoms is neglected and the two f functions on second-row atoms are replaced by a single f function taken from the cc-pVTZ basis set.[80] However, while the cost of the Δr^{CV} contribution is negligible in the framework of the original PCS2 model, it increases by about 3 times the cost of PCS3D computations. The way toward a cheaper model is paved by the unsupervised detection of bonded atoms and by the general finding that CV correlation affects only bond lengths, whereas its role is negligible for valence and dihedral angles.[13] Bonded atoms can be easily identified employing covalent radii (r_i^{cov}, taken for instance from ref 81) and Pauling bond orders P_{ij}[82]

$$P_{ij} = \exp[(r_i^{cov} + r_j^{cov} - r_{ij})/0.3] \quad (4)$$

In eq 4, r_{ij} is the interatomic distance in Å and two atoms are considered bonded if P_{ij} is larger than 0.3 (which corresponds to a distance 0.35 Å longer than the sum of the covalent radii). While this approximation does not reduce per se the required computational resources, it has been shown that the Δr^{CV} correction is well approximated by a simple one-parameter function of the principal quantum numbers (n_i) of the involved atoms,[42] which can be possibly supplemented by a contribution (Δr^{VB}) for small inaccuracies in the treatment of valence electrons[83]

$$r^{PCSB} = r^{rDSD} + \Delta r^B \quad (5)$$

with

$$\Delta r^B = \Delta r^{CVB} + \Delta r^{VB} \quad (6)$$

where

$$\Delta r_{ij}^{CVB} = -k\sqrt{n_i n_j - 1}\,(r_i^{cov} + r_j^{cov}) \quad (7)$$

In the above equation, $k = 0.0011$[42] and vanishing corrections are rightly obtained for bonds between first-row atoms.

Then, the Δr^{VB} correction is employed for counterbalancing the slight overestimation of delocalization for all bonds except C−O

$$\Delta r_{ij}^{VB} = \Delta r_{ij}^{CVB}[\sqrt{|P_{ij} - 2|} - 1][1 - \delta(i, O) - \delta(j, O)$$
$$+ \delta(i, O)\delta(j, O)] \quad (8)$$

The final PCS model with bond corrections (PCSB) model, which employs Kronecker δs to tune the inclusion of the corrective terms for selected bonds and just one empirical parameter (k), has the same cost as the underlying DFT geometry optimization. In the present work, all the geometry optimizations have been performed with the Gaussian package,[84] whereas the computation of the final PCSB geometries has been implemented in the freely available Web site (https://www.skies-village.it/proxima/pcsbonds/).

Experimental rotational constants represent very specific fingerprints of molecular structures and have very high precision (from 6 to 10 significant digits). However, the ground state values derived from MW spectra must be subjected to several corrections before being used for structural determinations.[85] Therefore, the best realistic level of accuracy for molecules containing more than 2 or 3 atoms is of the order of 0.1% (1 MHz for a constant of 1 GHz).[86] As a consequence, in the following, rotational constants will be truncated to 0.1 MHz and equilibrium values will be derived from their experimental ground-state counterparts employing computed electronic (ΔB_τ^{el}) and vibrational (ΔB_τ^{vib}) contributions (where τ is one of the three principal inertia axes)[24]

$$B_\tau^0 = B_\tau^{eq} + \Delta B_\tau^{el} + \Delta B_\tau^{vib} \quad (9)$$

with

$$\Delta B_\tau^{el} = -B_\tau^{eq}\frac{m}{M_p}g_{\tau\tau} \quad (10)$$

where the rotational g tensor is expressed in units of the nuclear magneton, m is the electron mass, and M_p the proton mass. While ΔB_τ^{el} could be safely computed by hybrid density functionals using London orbitals, several test computations[26,42] have shown that its contribution is smaller than the target accuracy of the proposed computational approach, at least for the molecules considered in the present study. As a consequence, in the following, this contribution will be neglected. On the other hand, ΔB_τ^{vib} contains harmonic (ΔB_τ^{harm}), Coriolis (ΔB_τ^{Cor}), and anharmonic (ΔB_τ^{anh}) contributions, which can be obtained from harmonic frequencies (ω_i), Coriolis couplings (ζ_{ij}), and semidiagonal cubic force constants (f_{iij})[21,24]

$$\Delta B_\tau^{harm} = (B_\tau^{eq})^2 \sum_{\eta=x,y,z} \sum_{i=1}^{N} \frac{3(a_{i,\tau\eta})^2}{4\omega_i I_\eta^{eq}} \quad (11)$$

$$\Delta B_\tau^{Cor} = -(B_\tau^{eq})^2 \sum_{i=1}^{N-1} \sum_{j=i+1}^{N} \frac{(\zeta_{ij,\tau})^2(\omega_i - \omega_j)^2}{\omega_i\omega_j(\omega_i + \omega_j)} \quad (12)$$

$$\Delta B_\tau^{anh} = (B_\tau^{eq})^2 \pi\sqrt{\frac{c}{h}} \sum_{i=1}^{N} \sum_{j=1}^{N} \frac{f_{iij}a_{j,\tau\tau}}{\omega_j^{3/2}} \quad (13)$$

In the above equations, $a_{i,\tau\eta}$ is the derivative of the τ, η component of the inertia moment with respect to the ith normal coordinate, c is the speed of light, h is the Planck constant, and I_η^{eq} is the principal moment of inertia along the axis η. Let us recall that, at variance with the individual vibro−rotational interaction constants α_i, the overall vibrational correction ΔB_τ^{vib} does not contain any resonant term.[9]

The bottleneck of the whole computation is represented by the anharmonic contribution, B_τ^{anh}. Remarkably, accurate zero point energies (ZPEs) and anharmonic frequencies can be

Table 1. Comparison between the SE Equilibrium Rotational Constants and Their Counterparts Obtained by Different QC Methods for Prototypical Fragments of Steroid Hormones[a]

	parameter	SE[b]	B3	rDSD	PCSB	ΔB_{B3}^{vib}
benzene	B_a^{eq}	5728.4	5676.9	5713.7	5729.7	39.1
	MUE, MAX		51.5	14.7	1.4	
	MUE %, MAX %		0.90	0.26	0.02	
phenol	B_a^{eq}	5691.9	5640.0	5678.5	5694.8	41.4
	B_b^{eq}	2636.2	2609.0	2627.9	2635.9	17.0
	B_c^{eq}	1801.9	1783.8	1796.5	1801.9	12.0
	MUE		32.4	9.1	1.1	
	MAX		51.9	13.4	2.9	
	MUE %		0.98	0.28	0.02	
	MAX %		1.03	0.32	0.05	
cyclohexane	B_a^{eq}	4350.6	4288.5	4333.8	4349.0	44.5
	MUE, MAX		62.2	16.8	1.7	
	MUE %, MAX %		1.43	0.39	0.04	
cyclohexanol *anti*	B_a^{eq}	4332.5	4268.4	4315.7	4330.9	44.3
	B_b^{eq}	2235.7	2200.4	2224.2	2232.1	20.0
	B_c^{eq}	1624.8	1597.5	1616.6	1622.4	15.6
	MUE		42.3	12.2	2.5	
	MAX		64.1	16.8	3.6	
	MUE %		1.58	0.47	0.12	
	MAX %		1.68	0.52	0.16	
cyclopentanone	B_a^{eq}	6682.3	6600.2	6662.4	6685.9	62.2
	B_b^{eq}	3376.7	3330.4	3362.8	3376.0	25.2
	B_c^{eq}	2429.2	2391.4	2420.3	2429.5	18.8
	MUE		55.5	14.3	1.6	1.9
	MAX		82.1	19.9	3.6	4.1
	MUE %		1.39	0.36	0.03	
	MAX %		1.56	0.41	0.05	
t-2-decalone	B_a^{eq}	2244.8	2218.5	2237.0	2245.4	15.5
	B_b^{eq}	766.2	753.6	763.1	765.9	8.4
	B_c^{eq}	611.6	600.8	609.1	611.3	7.3
	MUE		16.5	4.4	0.4	
	MAX		26.3	7.8	0.6	
	MUE %		1.52	0.38	0.04	
	MAX %		1.76	0.40	0.04	

[a]All the values (except % errors) are given in MHz. [b]SE equilibrium rotational constants obtained from the experimental ground state rotational constants and the B3 vibrational corrections. Experimental data (truncated to 1 decimal figure) taken from refs 29 and 104−105106107 for benzene, phenol, cyclohexane, cyclohexanol, cyclopentanone, and *trans*-2-decalone, respectively.

computed in the framework of the vibrational perturbation theory to second order (VPT2),[25,87−95] employing the full cubic and semidiagonal quartic force field, which can be obtained by finite differences of analytical Hessians.[96,97] However, well tested scaling factors[98−101] provide sufficiently accurate ZPEs and vibrational frequencies from harmonic force fields. Then, the semidiagonal cubic force fields needed for the computation of vibrational corrections to rotational constants can be obtained by a much faster approach based on analytical gradients evaluated at geometries displaced along the different normal modes.[102] While further details about the theoretical development and implementation in a new standalone code will be provided in a forthcoming paper, this reduced-cost approach has been employed systematically in the present work in order to obtain with reasonable computer cost the vibrational corrections of the studied hormones, which contain about 50 atoms. In fact, the magnitude of vibrational corrections is typically between 0.3 and 1.0% of that of the corresponding equilibrium rotational constant. Since the accuracy of B3 ΔB_τ^{vib} contributions falls well within 5%,[26] the ensuing error of 0.05% on the rotational constants is more than acceptable. As we will see, equilibrium

rotational constants computed from PCSB equilibrium geometries in conjunction with B3 vibrational corrections (denoted by the PCSB//B3 acronym) draw closer to the sought accuracy of 0.1% on the ground vibrational state rotational constants of all the target molecules. Noted is that this accuracy is reached with computational resources comparable to those required by the models routinely employed for the semiquantitative interpretation of MW spectra, namely, a full geometry optimization at the MP2 (or double-hybrid DFT) level in conjunction with a triple-ζ basis set and an evaluation of harmonic frequencies (albeit through finite differences of analytical gradients) by a hybrid density functional in conjunction with a double-ζ basis set.

3. RESULTS AND DISCUSSION

Before analyzing in detail the target hormones, we investigated the reliability of different computational approaches for representative fragments, whose experimental rotational constants are available (see Table 1). The experimental MW spectrum of cyclohexanol revealed the presence of *gauche* (*g*) and *anti* (*a*) conformers of the structure with an equatorial OH moiety.[103] Since the *g* conformers showed non-negligible

Table 2. Comparison between SE and Computed Geometrical Parameters for Prototypical Fragments of Steroid Hormones[a]

	parameter	SE[b]	B3	rDSD	PCSB
benzene	r_{C-C}	1.3916	1.3980	1.3934	1.3914
	r_{C-H}	1.0799	1.0869	1.0838	1.0826
phenol	r_{C_1-O}	1.3639	1.3721	1.3666	1.3638
	$r_{C_1-C_2}$	1.3920	1.3985	1.3936	1.3916
	$r_{C_2-C_3}$	1.3901	1.3973	1.3931	1.3911
	$r_{C_3-C_4}$	1.3902	1.3963	1.3914	1.3894
	$r_{C_4-C_5}$	1.3917	1.3992	1.3945	1.3924
	$r_{C_5-C_6}$	1.3888	1.3943	1.3899	1.3880
	r_{O-H}	0.9594	0.9697	0.9611	0.9601
	$r_{C_2-H_7}$	1.0836	1.0887	1.0857	1.0845
	$r_{C_3-H_8}$	1.0809	1.0867	1.0836	1.0824
	$r_{C_3-H_8}$	1.0809	1.0867	1.0836	1.0824
	$r_{C_4-H_9}$	1.0796	1.0859	1.0827	1.0815
	$r_{C_5-H_{10}}$	1.0813	1.0867	1.0836	1.0824
	$r_{C_6-H_{11}}$	1.0797	1.0856	1.0829	1.0817
	$a_{C_2-C_1-O}$	122.44	122.53	122.48	122.48
	$a_{C_6-C_1-O}$	117.14	117.21	117.28	117.28
	$a_{C_1-C_2-C_3}$	119.65	119.68	119.70	119.70
	$a_{C_2-C_3-C_4}$	120.50	120.51	120.50	120.50
	$a_{C_3-C_4-C_5}$	119.32	119.28	119.30	119.30
	$a_{C_4-C_5-C_6}$	120.75	120.75	120.74	120.74
	a_{C_1-O-H}	108.91	109.78	109.08	109.08
	$a_{C_3-C_2-H_7}$	120.51	120.25	120.32	120.32
	$a_{C_4-C_3-H_8}$	120.16	120.21	120.18	120.18
	$a_{C_5-C_4-H_9}$	120.37	120.37	120.37	120.37
	$a_{C_6-C_5-H_{10}}$	119.29	119.26	119.28	119.28
	$a_{C_1-C_6-H_{11}}$	119.05	119.02	119.04	119.04
cyclohexane	r_{C-C}	1.5258	1.5361	1.5285	1.5259
	$r_{C-H_{ax}}$	1.0957	1.1008	1.0972	1.0957
	$r_{C-H_{eq}}$	1.0914	1.0979	1.0941	1.0926
	a_{C-C-C}	111.11	111.39	111.13	111.13
	$a_{C-C-H_{ax}}$	108.99	109.08	109.07	109.07
	$a_{C-C-H_{eq}}$	110.33	110.28	110.33	110.33
	$d_{C-C-C-C}$	55.73	54.97	55.69	55.69
MAX(r)			0.0103	0.0039	0.0027
MAX(a,d)			0.87	0.19	0.19
MUE(r)			0.0068	0.0024	0.0010
MUE(a,d)			0.19	0.05	0.05
RMSD(r)			0.0070	0.0026	0.0012
RMSD(a,d)			0.32	0.08	0.08

[a]Bond lengths in Å, valence and dihedral angles in degrees. [b]Data taken from ref 29 for benzene and phenol and from ref 105 for cyclohexane.

tunneling splitting, only the results for the *a* conformers are reported in Table 1. There and in the following, the computed equilibrium rotational constants are compared with their SE counterparts obtained by adding computed vibrational corrections to the experimental ground state rotational constants (B_τ^0).

The maximum and mean unsigned errors (MAX and MUE, respectively) together with their relative values (MAX % and MUE %) given in Table 1 show that the B3 equilibrium
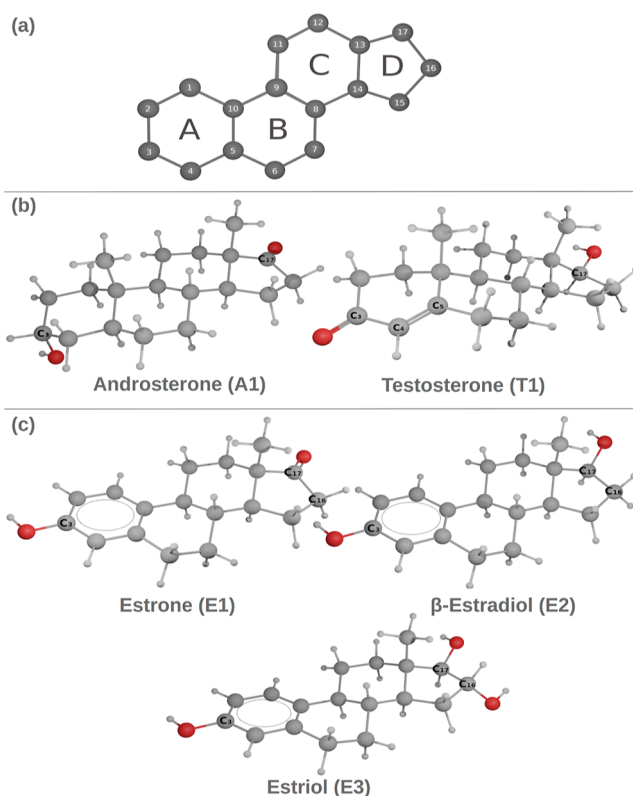
Figure 1. (a) Sterane or steroid backbone. The labeling follows the standard numbering system of the steroid nucleus.[60] (b) Molecular structures of androgens: androsterone and testosterone. (c) Molecular structures of estrogens: estrone, β-estradiol, and estriol.

rotational constants employed in the MW studies of steroid hormones[56−59] underestimate significantly the experimental values and, actually, a fortuitous error compensation improves the agreement when vibrational corrections are neglected. The rDSD model produces respectable results but underestimates systematically the SE rotational constants. This error is partially corrected by the Δr^B contribution (see eqs 5−8), which, however, produces variations of the rotational constants (ΔB^B) never exceeding 0.3% of the corresponding B_τ^{eq} value. At this level of accuracy, the vibrational corrections ΔB_τ^{vib} cannot be neglected since their contribution can reach 1% of the corresponding equilibrium values.

As expected, only PCSB equilibrium constants in conjunction with B3 vibrational corrections reach an accuracy well within the 0.1% target. As a matter of fact, without vibrational corrections, it would appear that rDSD and PCSB results are worse than their B3 counterparts, with this misleading conclusion pointing out that all the contributions to the overall experimental outcome need to be taken into account for an unbiased interpretation of experimental data. Since the new tool based on analytical gradients employed in the present paper for evaluating the vibrational corrections has the same cost as the underlying harmonic vibrational analysis, we strongly discourage the neglect of vibrational corrections in forthcoming studies.

A direct comparison between experimental and computed geometrical parameters would allow a more direct analysis of the performance of the PCSB model, but unfortunately, accurate experimental structures are not available for the quite large molecules, which are the main targets of the present study. However, accurate SE equilibrium geometries are available for
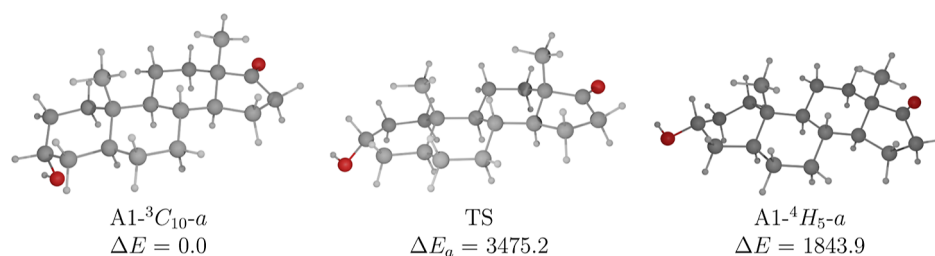
Figure 2. B3 optimized geometries and relative energies (in cm^{-1}, including ZPE contributions) of A1-$^3C_{10}$-a, A1-$^4H_5$-a, and the transition state (TS) ruling their interconversion.
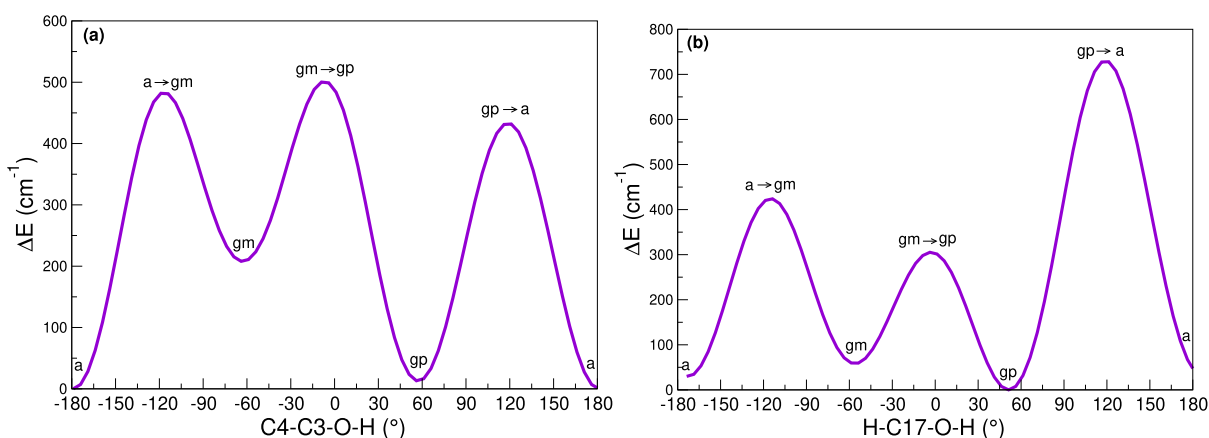
Figure 3. Potential energy surfaces (in cm^{-1}, at the B3 level) for (a) androsterone (A1), along the C4−C3−OH dihedral angle; (b) testosterone (T1), along the H−C17−OH dihedral angle.

Table 3. Relative Electronic Energies (ΔE), Activation Energies (ΔE_a), Enthalpies at 0 K (ΔH), Gibbs Free Energies at 448.15 K (ΔG), and Relative Populations at 448.15 K (% χ) of Androgens[a]

	ΔE_B	ΔE_{rDSD}	ΔE_a[b]	ΔH[c]	ΔG[d]	% χi
			Androsterone			
A1-$^3C_{10}$-a	0.0	0.0	$a \rightarrow gm$: 363.5	0.0	0.0	42.6
A1-$^3C_{10}$-gp	12.6	21.8	$gp \rightarrow a$: 263.6	21.2	22.5	39.6
A1-$^3C_{10}$-gm	207.7	291.5	$gm \rightarrow gp$: 120.8	286.8	272.5	17.8
			Testosterone			
T1-H_2^--gp	0.0	0.0	$gp \rightarrow a$: 620.4	0.0	0.0	37.4
T1-H_2^--a	29.7	57.1	$a \rightarrow gm$: 170.8	85.1	129.4	24.7
T1-H_2^--gm	58.2	63.3	$gm \rightarrow gp$: 86.1	51.6	39.3	32.9
T1-H_2^+-gp	516.5	483.1		534.5	624.4	5.0

[a]All data (except relative populations) are in cm^{-1}. The ordering of rotamers follows the ΔE_{rDSD} electronic energy. [b]Single point rDSD energies at B3 geometries, including ZPE_{B3} corrections. [c]$\Delta E_{rDSD} + ZPE_{B3}$. [d]$\Delta H + T\Delta S_{B3}$.
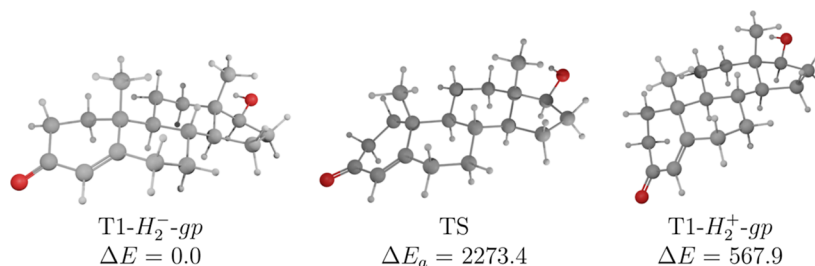
Figure 4. B3 optimized geometries and relative energies (in cm^{-1}, including ZPE contributions) of T1-H_2^--gp, T1-H_2^+-gp, and the transition state (TS) ruling their interconversion.

some of the basic building blocks, namely, benzene, phenol, and cyclohexane. The results collected in Table 2 show that the maximum difference, mean unsigned error, and root-mean-square deviation (MAX, MUE, and RMSD, respectively)

between PCSB and SE geometrical parameters are in the expected range and rival the accuracy of the much heavier composite wave function methods, which are not applicable to larger molecules.

Table 4. SE, B3, rDSD, and PCSB Equilibrium Rotational Constants (B_τ^{eq} in MHz), B3 Vibrational Corrections (ΔB_τ^{vib} in MHz), and Electric Dipole Moment Components (μ_τ in Debye) for the Most Stable Structures of Androsterone and Testosterone[a]

	parameter	SE[b]	B3	rDSD	PCSB	ΔB_{B3}^{vib}
			Androsterone			
A1-$^3C_{10}$-a	B_a^{eq}	744.3	734.3	740.6	743.5	8.9
	B_b^{eq}	175.7	173.0	175.0	175.6	1.7
	B_c^{eq}	161.5	159.1	160.9	161.5	1.4
	MUE		5.0	1.7	0.3	
	MAX		10.0	3.8	0.9	
	MUE %		1.46	0.44	0.1	
	MAX %		1.53	0.51	0.1	
	$|\mu_a|$		3.07	3.18		
	$|\mu_b|$		0.74	0.89		
	$|\mu_c|$		1.83	1.89		
			Testosterone			
T1-H_2^--gp	B_a^{eq}	793.4	786.7	788.8	791.9	8.1
	B_b^{eq}	170.3	167.6	169.6	170.2	1.6
	B_c^{eq}	155.2	152.6	154.6	155.2	1.4
	MUE		4.0	2.0	0.5	
	MAX		6.7	4.6	1.4	
	MUE %		1.37	0.44	0.1	
	MAX %		1.66	0.59	0.2	
	$|\mu_a|$		3.35	3.45		
	$|\mu_b|$		0.86	0.86		
	$|\mu_c|$		1.20	1.31		
T1-H_2^+-gp	B_a^{eq}		663.8	672.3	675.1	7.4
	B_b^{eq}		181.3	182.9	183.5	1.6
	B_c^{eq}		170.7	172.1	172.7	1.3
	$|\mu_a|$		2.97	3.13		
	$|\mu_b|$		0.57	0.54		
	$|\mu_c|$		2.19	2.15		

[a]Absolute mean and maximum unsigned errors between computed and experimental rotational constants (MUE and MAX in MHz) and the corresponding relative values (MUE % and MAX %) are also given. [b]SE equilibrium rotational constants obtained from the experimental ground state rotational constants and the B3 vibrational corrections. Experimental data (truncated to 1 decimal figure) taken from refs 56 and 57 for androsterone and testosterone, respectively.

The considered molecules are small enough to allow the computation of full cubic and semidiagonal quartic force fields by finite differences of analytical B3 Hessians. Then, the corresponding VPT2 anharmonic ZPEs were used to derive an average scaling factor for the harmonic ZPEs to be used in the case of hormones. It is reassuring that the obtained value (0.9870) is close to the value (0.9825) proposed in ref 99. The same data have been used to compare the semidiagonal cubic force fields obtained from finite differences of analytical gradients or analytical Hessians. The average and maximum relative differences of the vibrational corrections obtained by the two approaches (0.005 and 0.01%) are well within the target accuracy of the whole procedure.

Steroid hormones are a family of molecules derived from cholesterol that regulate many physiological processes, including the development and function of the reproductive system. Among them, two androgens [androsterone (A1)[56] and testosterone (T1)[57]] and two estrogens [estrone (E1)[58] and β-estradiol (E2)[59]] have been recently studied by microwave spectroscopy. As shown in Figure 1, the backbone of all steroid hormones is formed by three six-membered (A, B, and C) and

one five-membered (D) fused rings with a methyl group in position 13 and oxo- (A-E1) or hydroxy- (T-E2) substituents in position 17. The B, C, and D rings are always fully saturated, whereas the A ring is fully saturated (methyl-cyclohexanol in A1) or contains at most one double bond (methyl-cyclohexanone in T1) in androgens, but it is conjugated (phenol) in estrogens [E1, E2, and estriol (E3)]. Finally, E3 has one hydroxyl group also in position 16. Rings B and C always adopt a chair structure and ring D a nearly planar envelope structure, so that the main soft degrees of freedom concern the structure of ring A in androgens and the conformation of OH substituents in all hormones.

The rotational spectrum of androsterone (3α-hydroxy-5α-androstan-17-one, A1) has been recorded in the 2−8 GHz region by Caliebe et al.[56] A systematic search of low-energy structures evidenced the presence of chair ($^3C_{10}$) and half-chair ($^4H_5$) arrangements of the A ring, which were referred to as androsterone and p-androsterone, respectively, in ref 56. For each of those structures, the rotation around the C3−O bond can generate *anti* (*a*), *gauche*(+) (*gp*), and *gauche*(−) (*gm*) rotamers (referred to as the C$_4$−C$_3$−O−H dihedral angle). Only the A1-$^3C_{10}$-*a* species was detected in the experimental MW spectrum, and this finding is in full agreement with our QC computations, which indicate that the half-chair structure is about 1800 cm^{-1} less stable than its chair counterpart and that the energy barrier ruling the interconversion between these two structures is larger than 3000 cm^{-1} (see Figure 2). On the other hand, the different rotamers of the chair species have comparable stability but are separated by quite low-energy barriers (see Figure 3a and Table 3). As a consequence, when androsterone is heated at 448.15 K using a heatable reservoir, all three rotamers are populated (see % χ_i in Table 3), but, when the gas is expanded the *gauche*(+) and *gauche*(−) rotamers relax to the *anti* rotamer, overcoming energy barriers (364 or 264 cm^{-1}, see Table 3) lower than the threshold value of about 400 cm^{-1}.[72−74]

The MW spectrum of testosterone (17β-hydroxyandrost-4-ene-3-one, T1) has been recorded by the LA-CP-FTMW technique[57] in the 1.5−6.5 GHz range. In this case, the lowest energy minima correspond to the H_2^- and H_2^+ structures (I and II, according to the nomenclature of ref 57) due to the presence of a double bond in the A ring. In configuration I, the A ring takes a half-chair disposition and lies almost in the same plane as rings B−D, so that the molecule adopts an extended form. Configuration II is, instead, in a semifolded arrangement, with the A ring almost perpendicular to the average plane of the other rings (see Figure 4). The interconversion between these two structures is hampered by an energy barrier higher than 2000 cm^{-1}, while the population of the less stable species (about 5%, see Table 3) is at the limit of MW detectability.

Three staggered orientations (*a*, *gp*, and *gm*) are possible for the OH moiety in position 17, which are separated by low-energy barriers (see Figure 3b and Table 3). In analogy with androsterone, heating of testosterone produces non-negligible populations of all those rotamers (see % χ_i in Table 3), but the successive gas expansion leads to the relaxation of the *anti* and *gauche*(−) rotamers to their more stable *gauche*(+) counterpart, overcoming energy barriers (171 and/or 86 cm^{-1}) lower than the threshold value of about 400 cm^{-1}.[72−74]

The experimental rotational constants of the single species of androsterone and testosterone detected in the MW spectra are compared with their computed counterparts in Table 4. In order to separate geometric and vibrational effects, the B3 vibrational
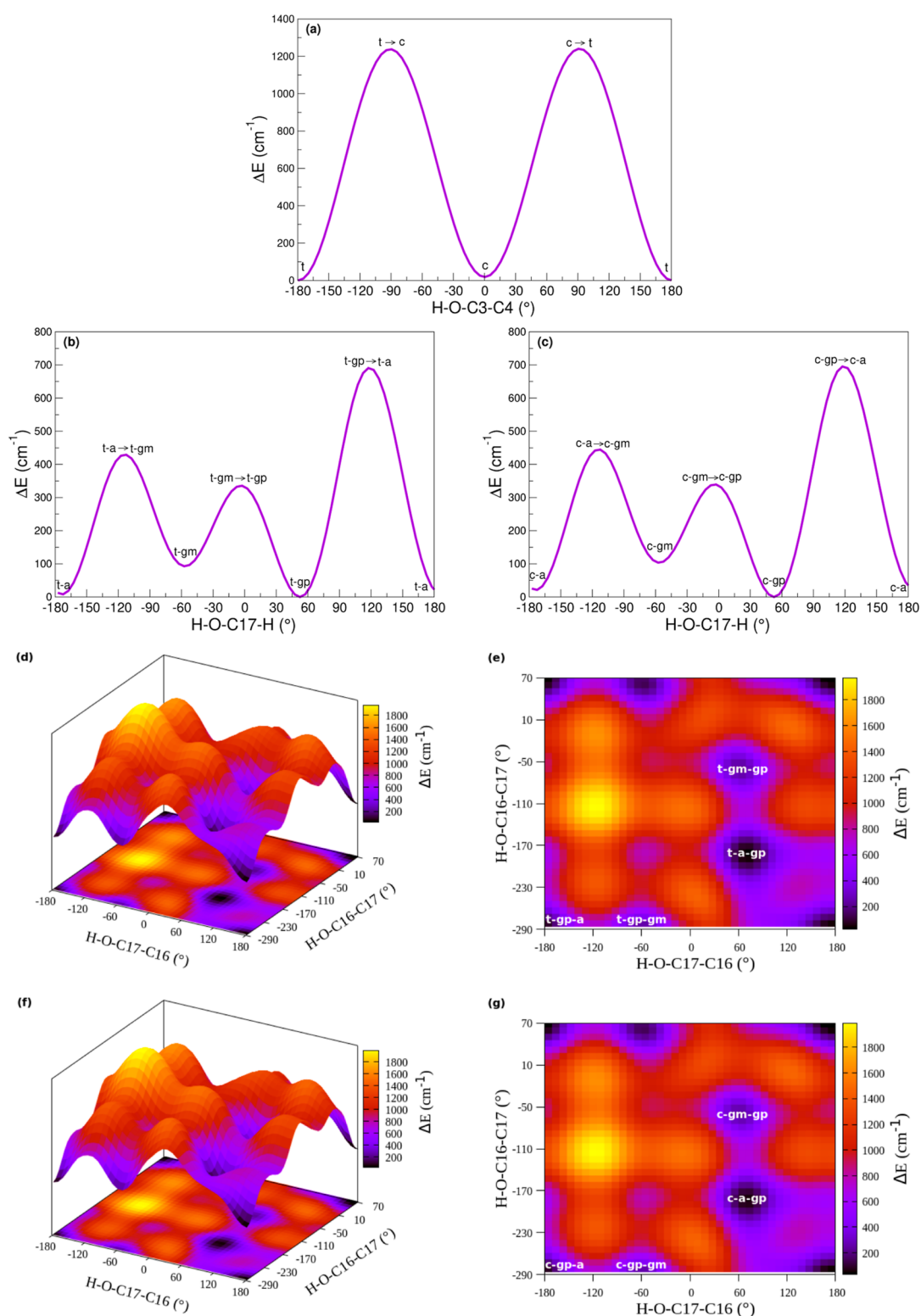
Figure 5. Potential energy surfaces (in cm^{-1}, at the B3 level) for (a) estrone (E1), along the H−O−C3−C4 dihedral angle; (b,c) *trans* and *cis* β-estradiol (E2), respectively, along the H−O−C17−H dihedral angle; (d,e) *trans*-estriol and (f,g) *cis*-estriol along the H−O−C17−C16 and H−O−C16−C17 dihedral angles, respectively.

corrections have been employed to estimate SE equilibrium rotational constants. It is quite apparent that those corrections cannot be neglected for an unbiased comparison between theory and experiment. Furthermore, rDSD results represent a significant improvement with respect to B3 values, and the

PCSB model reaches the sought 0.1% accuracy for both hormones.

Estradiol, estrone, and estriol are the three major forms of estrogen hormones in women, and they are responsible for the female reproductive system. While the first two hormones were studied in the gas phase by MW spectroscopy, this is not the case

Table 5. Relative Electronic Energies (ΔE), Activation Energies (ΔE_a), Enthalpies at 0 K (ΔH), Gibbs Free Energies (ΔG), and Relative Populations (χ %) at 468.15 K for E1 and E2, and at 563.15 K for E3[d]

	ΔE_{B3}	ΔE_{rDSD}	ΔE_a[a]	ΔH[b]	ΔG[c]	% χ_i
			Estrone			
t-E1	0.0	0.0	$t \to c$: 1033.0	0.0	0.0	51.7
c-E1	18.5	15.1		20.1	21.0	48.3
			β-Estradiol			
c-E2-gp	0.0	0.0	$c\text{-}gp \to c\text{-}a$: 745.1	0.0	7.3	19.6
t-E2-gp	2.6	3.3	$t\text{-}gp \to t\text{-}a$: 747.3	10.7	0.0	20.0
t-E2-a	10.3	38.6	$t\text{-}a \to t\text{-}gm$: 356.2	66.8	110.5	14.0
c-E2-a	20.9	46.8	$c\text{-}a \to c\text{-}gm$: 357.0	81.2	128.0	13.3
t-E2-gm	95.2	93.3	$t\text{-}gm \to t\text{-}gp$: 242.4	76.4	52.5	16.9
c-E2-gm	103.3	98.9	$c\text{-}gm \to c\text{-}gp$: 237.4	87.7	66.0	16.2
			Estriol			
t-E3-a-gp	0.0	0.0	$t\text{-}a\text{-}gp \to t\text{-}gm\text{-}gp$: 506.6	0.0	9.2	17.5
c-E3-a-gp	8.7	8.3	$c\text{-}a\text{-}gp \to c\text{-}gm\text{-}gp$: 512.0	13.7	0.0	18.0
t-E3-gp-a	27.3	32.8	$t\text{-}gp\text{-}ga \to t\text{-}gp\text{-}gm$: 538.9	31.3	26.8	16.5
c-E3-gp-a	41.8	32.8	$c\text{-}gp\text{-}a \to c\text{-}gp\text{-}gm$: 523.1	39.3	34.2	16.2
c-E3-gp-gm	129.0	155.8		193.9	247.6	8.1
t-E3-gp-gm	131.7	157.6		188.3	260.5	7.8
t-E3-gm-gp	217.8	249.0		244.7	249.7	8.1
c-E3-gm-gp	228.4	256.9		258.4	266.0	7.7

[a]Single point rDSD energies at B3 geometries, including ZPE_{B3} corrections, for transition states involving rotations of a single dihedral angle. [b]ΔE_{rDSD} + ZPE$_{B3}$. [c]ΔH + $T\Delta S_{B3}$. [d]All data (except relative populations) are in cm^{-1}. The ordering of rotamers follows the ΔE_{rDSD} electronic energy.

Table 6. SE, B3, rDSD, and PCSB Equilibrium Rotational Constants (B_τ^{eq} in MHz), B3 Vibrational Corrections (ΔB_τ^{vib} in MHz), B3, and rDSD Electric Dipole Moment Components (μ_τ in Debye) for the Two Most Stable Structures of Estrone[a]

	parameter	SE[b]	B3	rDSD	PCSB	ΔB_{B3}^{vib}
t-E1	B_a^{eq}	946.9	936.8	944.7	948.2	8.6
	B_b^{eq}	181.1	178.6	180.3	180.9	1.5
	B_c^{eq}	160.4	158.2	159.7	160.3	1.2
	MUE		4.9	1.2	0.5	
	MAX		10.1	2.2	1.3	
	MUE %		1.26	0.36	0.1	
	MAX %		1.37	0.44	0.1	
	$|\mu_a|$		1.88	1.89		
	$|\mu_b|$		0.98	1.16		
	$|\mu_c|$		0.41	0.45		
c-E1	B_a^{eq}	946.4	936.4	944.3	947.8	8.5
	B_b^{eq}	181.0	178.6	180.2	180.8	1.5
	B_c^{eq}	160.4	158.2	159.7	160.2	1.2
	MUE		4.9	1.2	0.6	
	MAX		10.0	2.1	1.4	
	MUE %		1.26	0.36	0.1	
	MAX %		1.37	0.45	0.1	
	$|\mu_a|$		1.66	1.72		
	$|\mu_b|$		3.65	3.71		
	$|\mu_c|$		0.79	0.78		

[a]Absolute mean and maximum unsigned errors between computed and experimental rotational constants (MUE and MAX in MHz) and the corresponding relative values (MUE % and MAX %) are also given. [b]SE equilibrium rotational constants obtained from the experimental ground state rotational constants and the B3 vibrational corrections. Experimental data (truncated to 1 decimal figure) taken from ref 58.

of the remarkable agreement between theory and experiments for estrone and estradiol. In all the three hormones, the replacement of the saturated A ring with phenol leads to significant barriers opposing the rotation of the OH group at C3 out of the two nearly isoenergetic *cis* (*c*) and *trans* (*t*) minima (see Figure 5 and Table 5). As a consequence, two structures should be (and have actually been) detected in the MW spectrum of estrone (3-hydroxyestra-1,3,5(10)-triene-17-one, E1), which does not have any additional soft dihedral angle.[58]

The experimental rotational constants of the two structures of estrone detected in the MW spectra are compared with their computed counterparts in Table 6, with B3 vibrational corrections being employed to estimate SE equilibrium rotational constants. Once again the rDSD results represent significant improvements with respect to B3 values, and the PCSB model reaches the sought 0.1% accuracy.

The β-estradiol hormone (estra-1,3,5(10)-triene-3,17β-diol) has been studied by laser[71] and MW[59] spectroscopy, employing in both cases a jet expansion. The rotational spectrum was collected in the same way as that for androsterone, with an extension to 18 GHz. Morishima et al.[71] have reported six stable rotamers (listed in Table 5) corresponding to the *a*, *gp*, and *gm* conformers of the OH group at C17 for each of the *c* and *t* structures of phenol discussed above. Four of these structures have been observed by laser spectroscopy, and three of them have been detected by MW spectroscopy. All of the conformers show very similar rotational constants because of the identical steroidal backbone and the weak effect on the overall mass distribution of the change in the orientation of only the two hydroxy groups, despite their significant distance from the molecular center of mass. However, changes in the relative orientations of the hydroxy groups can lead to major changes in the dipole-moment components, which determine the transition strengths in MW spectra.[108]

The computed energy barriers ruling the interconversion between different structures suggest that *gp* rotamers can easily

for the third one. However, the results of the present QC study of estriol should provide valuable pieces of information in view

Table 7. SE, B3, rDSD, and PCSB Equilibrium Rotational Constants (B_τ^{eq} in MHz), B3 Vibrational Corrections (ΔB_τ^{vib} in MHz), B3, and rDSD Electric Dipole Moment Components (μ_τ in Debye) for the Most Stable Structures of β-Estradiol Not Involved in Fast Relaxation Processes[a]

	parameter	SE[b]	B3	rDSD	PCSB	ΔB_{B3}^{vib}
t-E2-gp	B_a^{eq}	948.4	937.9	946.0	949.6	8.6
	B_b^{eq}	176.3	173.8	175.5	176.1	1.5
	B_c^{eq}	156.6	154.4	155.9	156.5	1.3
	MUE		5.0	1.3	0.5	
	MAX		10.4	2.4	1.2	
	MUE %		1.30	0.38	0.1	
	MAX %		1.41	0.45	0.1	
	$\|\mu_a\|$		0.68	0.51		
	$\|\mu_b\|$		1.53	1.40		
	$\|\mu_c\|$		1.10	1.14		
t-E2-a	B_a^{eq}		934.8	943.0	946.5	8.7
	B_b^{eq}		174.0	175.7	176.3	1.5
	B_c^{eq}		154.5	156.0	156.6	1.3
	$\|\mu_a\|$		0.48	0.32		
	$\|\mu_b\|$		0.09	0.18		
	$\|\mu_c\|$		0.62	0.55		
c-E2-gp	B_a^{eq}	947.9	937.8	945.8	949.3	8.6
	B_b^{eq}	176.3	173.8	175.5	176.1	1.5
	B_c^{eq}	156.6	154.4	155.9	156.4	1.3
	MUE		5.0	1.2	0.6	
	MAX		10.1	2.1	1.5	
	MUE %		1.30	0.38	0.1	
	MAX %		1.43	0.47	0.2	
	$\|\mu_a\|$		0.47	0.31		
	$\|\mu_b\|$		1.14	1.11		
	$\|\mu_c\|$		0.68	0.74		
c-E2-a	B_a^{eq}	945.1	934.4	942.7	946.2	8.5
	B_b^{eq}	176.4	174.0	175.6	176.2	1.5
	B_c^{eq}	156.7	154.5	156.0	156.6	1.3
	MUE		5.1	0.8	0.4	
	MAX		10.7	0.9	1.0	
	MUE %		1.30	0.35	0.1	
	MAX %		1.40	0.51	0.1	
	$\|\mu_a\|$		0.27	0.12		
	$\|\mu_b\|$		2.77	2.69		
	$\|\mu_c\|$		1.04	0.94		

[a]Absolute mean and maximum unsigned errors between computed and experimental rotational constants (MUE and MAX in MHz) and the corresponding relative values (MUE % and MAX %) are also given. [b]SE equilibrium rotational constants obtained from the experimental ground state rotational constants and the B3 vibrational corrections. Experimental data (truncated to 1 decimal figure) taken from ref 59.

Table 8. B3, rDSD, and PCSB Equilibrium Rotational Constants (B_τ^{eq} in MHz) and B3 Vibrational Corrections ($\Delta B_t au^{vib}$ in MHz) for the Most Stable Structures of Estriol

	parameter	B3	rDSD	PCSB	ΔB_{B3}^{vib}
t-E3-gp-a	B_a^{eq}	849.3	857.1	860.2	9.0
	B_b^{eq}	151.6	153.1	153.6	1.3
	B_c^{eq}	135.5	136.8	137.2	1.1
t-E3-gp-gm	B_a^{eq}	843.9	851.8	854.9	8.7
	B_b^{eq}	152.0	153.4	153.9	1.3
	B_c^{eq}	135.7	137.0	137.5	1.1
t-E3-a-gp	B_a^{eq}	848.4	855.7	858.8	9.3
	B_b^{eq}	151.9	153.4	153.9	1.3
	B_c^{eq}	135.8	137.1	137.6	1.1
t-E3-gm-gp	B_a^{eq}	849.1	857.0	860.2	8.6
	B_b^{eq}	151.6	153.1	153.6	1.3
	B_c^{eq}	135.5	136.8	137.2	1.2
c-E3-gp-a	B_a^{eq}	849.2	857.0	860.1	9.0
	B_b^{eq}	151.6	153.0	153.6	1.3
	B_c^{eq}	135.5	136.8	137.2	1.1
c-E3-gp-gm	B_a^{eq}	843.7	851.7	854.8	8.6
	B_b^{eq}	151.9	153.4	153.9	1.3
	B_c^{eq}	135.7	137.0	137.5	1.1
c-E3-a-gp	B_a^{eq}	848.4	855.5	858.7	9.3
	B_b^{eq}	151.9	153.3	153.9	1.3
	B_c^{eq}	135.8	137.1	137.6	1.1
c-E3-gm-gp	B_a^{eq}	849.0	856.9	860.1	8.6
	B_b^{eq}	151.6	153.0	153.6	1.3
	B_c^{eq}	135.5	136.8	137.2	1.2

fast relaxation processes gives strong support to the overall picture emerging from QC computations.

Estriol (estra-1,3,5(10)-triene-3,16α, 17β-triol) has an additional OH group at position 16. In this case, 18 rotamers are, in principle, possible, 9 each for the c and t conformer of the phenol ring. Among them, the 8 low-energy minima reported in Table 5 survived after full geometry optimizations starting from the guesses provided by two-dimensional relaxed scans (see Figure 5d−g). All of those structures could be, in principle, detectable in MW spectra since all the relaxation processes are ruled by energy barriers higher than 400 cm^{-1}. The corresponding rotational constants computed by different QC approaches are collected in Table 8, together with the activation energies ruling interconversion processes involving a single dihedral angle. However, the computed dipole moment components of the t-E3-gp-gm and c-E3-gm-gp species are very low (see Table S4), so that only the other six rotamers of estriol could be actually detectable.

4. CONCLUSIONS

A general computational workflow aimed at an accurate description of the structural and spectroscopic properties of biomolecule building blocks has been applied to a panel of steroid hormones. Accurate structures and relative energies were obtained by employing a last-generation double-hybrid functional in conjunction with a triple-ζ basis set. Then, ground state rotational constants were obtained at the PCSB//B3 level. The agreement between computed and experimental results for all the studied hormones permits the unbiased interpretation of the latter in terms of well-defined stereoelectronic effects. Work is in progress in our laboratories to extend this approach to other physical−chemical properties, to large-amplitude motions, and to molecules containing heavy atoms.[109] However, even

relax to their more stable gm counterparts for both the c and t conformers. However, this is not the case for a rotamers in view of the quite high energy barriers governing their conversion to other rotamers (see Table 5).

As a consequence, four species are expected to have significant populations in the jet, in agreement with the results of laser spectroscopy. On the other hand, the very low dipole moment components computed for the ta species (see Table 7) suggest that it could escape unequivocal detection in MW experiments. Furthermore, the remarkable agreement between the computed and experimental rotational constants collected in the same Table for the remaining three low-energy species not involved in

pending these further developments, the results of the present paper and of previous related studies[14,55,66,83] provide a general panorama of prototypical molecular bricks of life and pave the way toward accurate studies of molecules containing few dozen atoms also by nonspecialists.

■ ASSOCIATED CONTENT

ⓢ Supporting Information

The Supporting Information is available free of charge at https://pubs.acs.org/doi/10.1021/acs.jpca.4c00573.

> Additional data for the hormone structures not detected in MW spectra including equilibrium rotational constants and vibrational corrections for androsterone, testosterone, and β-estradiol, electric dipole moment components for estriol, and PCSB geometries of all the energy minima for fragments of steroid hormones, androsterone, testosterone, estrone, β-estradiol, and estriol (PDF)

■ AUTHOR INFORMATION

Corresponding Author

Vincenzo Barone — *INSTM, 50121 Firenze, Italy;* ⓞ orcid.org/0000-0001-6420-4107; Email: vincebarone52@gmail.com

Authors

Lina Uribe — *Scuola Normale Superiore di Pisa, 56126 Pisa, Italy; Scuola Superiore Meridionale, 80138 Napoli, Italy*

Silvia Di Grande — *Scuola Normale Superiore di Pisa, 56126 Pisa, Italy; Scuola Superiore Meridionale, 80138 Napoli, Italy;* ⓞ orcid.org/0000-0002-6550-0220

Luigi Crisci — *Scuola Normale Superiore di Pisa, 56126 Pisa, Italy*

Federico Lazzari — *Scuola Normale Superiore di Pisa, 56126 Pisa, Italy;* ⓞ orcid.org/0000-0003-4506-3200

Marco Mendolicchio — *Scuola Normale Superiore di Pisa, 56126 Pisa, Italy;* ⓞ orcid.org/0000-0002-4504-853X

Complete contact information is available at: https://pubs.acs.org/10.1021/acs.jpca.4c00573

Notes

The authors declare no competing financial interest.

■ ACKNOWLEDGMENTS

■ REFERENCES

(1) Levine, I. *Molecular Spectroscopy*; Wiley, 1975.

(2) Cleeton, C. E.; Williams, N. H. Electromagnetic Waves of 1.1 cm Wave-Length and the Absorption Spectrum of Ammonia. *Phys. Rev.* **1934**, *45*, 234−237.

(3) *Atomic and Molecular Beam Methods*; Schols, G., Bassi, D., Buck, U., Eds.; Oxford University Press, 1988.

(4) Alonso, J. L.; López, J. C. In *Gas-Phase IR Spectroscopy and Structure of Biological Molecules*; Rijs, A. M., Oomens, J., Eds.; Springer International Publishing: Cham, 2015; pp 335−401.

(5) Alonso, J. L.; Perez, C.; Eugenia Sanz, M.; Lopez, J. C.; Blanco, S. Seven Conformers of l-Threonine in the Gas Phase: a LA-MB-FTMW Study. *Phys. Chem. Chem. Phys.* **2009**, *11*, 617−627.

(6) Bermúdez, C.; Mata, S.; Cabezas, C.; Alonso, J. L. Tautomerism in Neutral Histidine. *Angew. Chem., Int. Ed. Engl.* **2014**, *53*, 11015.

(7) Mata, S.; Peña, I.; Cabezas, C.; López, J.; Alonso, J. L. A Broadband Fourier-Transform Microwave Spectrometer With Laser Ablation Source: The Rotational Spectrum of Nicotinic Acid. *J. Mol. Spectrosc.* **2012**, *280*, 91−96.

(8) Schmitz, D.; Alvin Shubert, V.; Betz, T.; Schnell, M. Multi-Resonance Effects Within a Single Chirp in Broadband Rotational Spectroscopy: The Rapid Adiabatic Passage Regime for Benzonitrile. *J. Mol. Spectrosc.* **2012**, *280*, 77−84.

(9) Puzzarini, C.; Stanton, J. F.; Gauss, J. Quantum-Chemical Calculation of Spectroscopic Parameters for Rotational Spectroscopy. *Int. Rev. Phys. Chem.* **2010**, *29*, 273−367.

(10) Barone, V.; Alessandrini, S.; Biczysko, M.; Cheeseman, J. R.; Clary, D. C.; McCoy, A. B.; DiRisio, R. J.; Neese, F.; Melosso, M.; Puzzarini, C. Computational Molecular Spectroscopy. *Nat. Rev. Methods Primers* **2021**, *1*, 38.

(11) Puzzarini, C.; Stanton, J. F. Connections Between the Accuracy of Rotational Constants and Equilibrium Molecular Structures. *Phys. Chem. Chem. Phys.* **2023**, *25*, 1421−1429.

(12) Mancini, G.; Fusè, M.; Lazzari, F.; Barone, V. Fast Exploration of Potential Energy Surfaces with a Joint Venture of Quantum Chemistry, Evolutionary Algorithms and Unsupervised Learning. *Digital Discovery* **2022**, *1*, 790−805.

(13) Puzzarini, C.; Barone, V. Diving for Accurate Structures in the Ocean of Molecular Systems with the Help of Spectroscopy and Quantum Chemistry. *Acc. Chem. Res.* **2018**, *51*, 548−556.

(14) Barone, V.; Puzzarini, C. Gas-Phase Computational Spectroscopy: The Challenge of the Molecular Bricks of Life. *Annu. Rev. Phys. Chem.* **2023**, *74*, 29−52.

(15) Puzzarini, C.; Bloino, J.; Tasinato, N.; Barone, V. Accuracy and Interpretability: The Devil and the Holy Grail. New Routes Across Old Boundaries in Computational Spectroscopy. *Chem. Rev.* **2019**, *119*, 8131−8191.

(16) Heim, Z. N.; Amberger, B. K.; Esselman, B. J.; Stanton, J. F.; Woods, R. C.; McMahon, R. J. Molecular Structure Determination: Equilibrium Structure of Pyrimidine from Rotational Spectroscopy (r_e^{SE})and High-Level Ab Initio Calculation (r_e) Agree Within the Uncertainty of Experimental Measurement. *J. Chem. Phys.* **2020**, *152*, 104303.

(17) Warden, C. E.; Smith, D. G. A.; Burns, L. A.; Bozkaya, U.; Sherrill, C. D. Efficient and automated computation of accurate molecular geometries using focal-point approximations to large-basis coupled-cluster theory. *J. Chem. Phys.* **2020**, *152*, 124109.

(18) Watrous, A.; Westbrook, B. R.; Fortenberry, R. C. F12-TZ-cCR: A Methodology for Faster and Still Highly Accurate Quartic Force Fields. *J. Phys. Chem. A* **2021**, *125*, 10532−10540.

(19) Pulay, P.; Meyer, W.; Boggs, J. E. Cubic Force Constants and Equilibrium Geometry of Methane From Hartree−Fock and Correlated Wavefunctions. *J. Chem. Phys.* **1978**, *68*, 5077−5085.

(20) Pawłowski, F.; Jørgensen, P.; Olsen, J.; Hegelund, F.; Helgaker, T.; Gauss, J.; Bak, K. L.; Stanton, J. F. Molecular Equilibrium Structures From Experimental Rotational Constants and Calculated Vibration−Rotation Interaction Constants. *J. Chem. Phys.* **2002**, *116*, 6482−6496.

(21) Demaison, J. Experimental, semi-experimental andab initioequilibrium structures. *Mol. Phys.* **2007**, *105*, 3109−3138.

(22) Demaison, J.; Boggs, J. E.; Császár, A. G. *Equilibrium Molecular Structures: from Spectroscopy to Quantum Chemistry*; CRC Press, 2016.

(23) Penocchio, E.; Mendolicchio, M.; Tasinato, N.; Barone, V. Structural Features of the Carbon−Sulfur Chemical Bond: a Semi-Experimental Perspective. *Can. J. Chem.* **2016**, *94*, 1065−1076.

(24) Mendolicchio, M.; Penocchio, E.; Licari, D.; Tasinato, N.; Barone, V. Development and Implementation of Advanced Fitting Methods for the Calculation of Accurate Molecular Structures. *J. Chem. Theory Comput.* **2017**, *13*, 3060−3075.

(25) Mendolicchio, M. Harnessing the power of curvilinear internal coordinates: from molecular structure prediction to vibrational spectroscopy. *Theor. Chem. Acc.* **2023**, *142*, 133.

(26) Piccardo, M.; Penocchio, E.; Puzzarini, C.; Biczysko, M.; Barone, V. Semi-Experimental Equilibrium Structure Determinations by Employing B3LYP/SNSD Anharmonic Force Fields: Validation and Application to Semirigid Organic Molecules. *J. Phys. Chem. A* **2015**, *119*, 2058−2082.

(27) Penocchio, E.; Piccardo, M.; Barone, V. Semiexperimental Equilibrium Structures for Building Blocks of Organic and Biological

Molecules: The B2PLYP Route. *J. Chem. Theory Comput.* **2015**, *11*, 4689−4707.

(28) Melli, A.; Tonolo, F.; Barone, V.; Puzzarini, C. Extending the Applicability of the Semi-Experimental Approach by Means of "Template Molecule" and "Linear Regression" Models on Top of DFT Computations. *J. Phys. Chem. A* **2021**, *125*, 9904−9916.

(29) Ceselin, G.; Barone, V.; Tasinato, N. Accurate Biomolecular Structures by the Nano-LEGO Approach: Pick the Bricks and Build Your Geometry. *J. Chem. Theory Comput.* **2021**, *17*, 7290−7311.

(30) Barone, V.; Ceselin, G.; Lazzari, F.; Tasinato, N. Toward Spectroscopic Accuracy for the Structures of Large Molecules at DFT Cost: Refinement and Extension of the Nano-LEGO Approach. *J. Phys. Chem. A* **2023**, *127*, 5183−5192.

(31) Shavitt, I.; Bartlett, R. J. *Many-Body Methods in Chemistry and Physics: MBPT and Coupled-Cluster Theory*; Cambridge University Press, 2009.

(32) Agbaglo, D.; Fortenberry, R. C. The performance of explicitly correlated methods for the computation of anharmonic vibrational frequencies. *Int. J. Quantum Chem.* **2019**, *119*, No. e25899.

(33) Ye, H.; Mendolicchio, M.; Kruse, H.; Puzzarini, C.; Biczysko, M.; Barone, V. The Challenging Equilibrium Structure of HSSH: Another Success of the Rotational Spectroscopy/Quantum Chemistry Synergism. *J. Mol. Struct.* **2020**, *1211*, 127933.

(34) Barone, V. Accuracy Meets Feasibility for the Structures and Rotational Constants of the Molecular Bricks of Life: A Joint Venture of DFT and Wave-Function Methods. *J. Phys. Chem. Lett.* **2023**, *14*, 5883−5890.

(35) Barone, V.; Crisci, L.; Di Grande, S. Accurate Thermochemical and Kinetic Parameters at Affordable Cost by Means of the Pisa Composite Scheme (PCS). *J. Chem. Theory Comput.* **2023**, *19*, 7273−7286.

(36) Teale, A. M.; Helgaker, T.; Savin, A.; Adamo, C.; Aradi, B.; Arbuznikov, A. V.; Ayers, P. W.; Baerends, E. J.; Barone, V.; Calaminici, P.; et al. DFT Exchange: Sharing Perspectives on the Workhorse of Quantum Chemistry and Materials Science. *Phys. Chem. Chem. Phys.* **2022**, *24*, 28700−28781.

(37) Møller, C.; Plesset, M. S. Note on an Approximation Treatment for Many-Electron Systems. *Phys. Rev.* **1934**, *46*, 618−622.

(38) Alessandrini, S.; Barone, V.; Puzzarini, C. Extension of the "Cheap" Composite Approach to Noncovalent Interactions: The jun-ChS Scheme. *J. Chem. Theory Comput.* **2020**, *16*, 988−1006.

(39) Lupi, J.; Alessandrini, S.; Puzzarini, C.; Barone, V. JunChS and JunChS-F12 Models: Parameter-Free Efficient Yet Accurate Composite Schemes For Energies and Structures of Noncovalent Complexes. *J. Chem. Theory Comput.* **2021**, *17*, 6974−6992.

(40) Barone, V.; Di Grande, S.; Lazzari, F.; Mendolicchio, M. Accurate Structures and Spectroscopic Parameters of Guanine Tautomers in the Gas Phase by the Pisa Conventional and Explicitly Correlated Composite Schemes (PCS and PCS-F12). *J. Phys. Chem. A* **2023**, *127*, 6771−6778.

(41) Di Grande, S.; Kállay, M.; Barone, V. Accurate Thermochemistry at Affordable Cost by Means of an Improved Version of the JunChS-F12 Model Chemistry. *J. Comput. Chem.* **2023**, *44*, 2149−2157.

(42) Barone, V. PCS/Bonds and PCS0: Pick Your Molecule and Get Its Accurate Structure and Ground State Rotational Constants at DFT Cost. *J. Chem. Phys.* **2023**, *159*, 081102.

(43) Caldeweyher, E.; Ehlert, S.; Hansen, A.; Neugebauer, H.; Spicher, S.; Bannwarth, C.; Grimme, S. A Generally Applicable Atomic-Charge Dependent London Dispersion Correction. *J. Chem. Phys.* **2019**, *150*, 154122.

(44) Santra, G.; Sylvetsky, N.; Martin, J. M. Minimally Empirical Double-Hybrid Functionals Trained Against the GMTKN55 Database: revDSD-PBEP86-D4, revDOD-PBE-D4, and DOD-SCAN-D4. *J. Phys. Chem. A* **2019**, *123*, 5129−5143.

(45) Biczysko, M.; Panek, P.; Scalmani, G.; Bloino, J.; Barone, V. Harmonic and Anharmonic Vibrational Frequency Calculations with the Double-Hybrid B2PLYP Method: Analytic Second Derivatives and Benchmark Studies. *J. Chem. Theory Comput.* **2010**, *6*, 2115−2125.

(46) Becke, A. D. Density-Functional Exchange-Energy Approximation with Correct Asymptotic Behavior. *Phys. Rev. A* **1988**, *38*, 3098−3100.

(47) Lee, C.; Yang, W.; Parr, R. G. Development of the Colle-Salvetti Correlation-Energy Formula Into a Functional of the Electron Density. *Phys. Rev. B* **1988**, *37*, 785−789.

(48) Becke, A. D. Density-Functional Thermochemistry. III. The Role of Exact Exchange. *J. Chem. Phys.* **1993**, *98*, 5648−5652.

(49) Grimme, S.; Antony, J.; Ehrlich, S.; Krieg, H. A Consistent and Accurate Ab Initio Parametrization of Density Functional Dispersion Correction (DFT-D) for the 94 Elements H-Pu. *J. Chem. Phys.* **2010**, *132*, 154104.

(50) Grimme, S.; Ehrlich, S.; Goerigk, L. Effect of the Damping Function in Dispersion Corrected Density Functional Theory. *J. Comput. Chem.* **2011**, *32*, 1456−1465.

(51) Hehre, W. J.; Ditchfield, R.; Pople, J. A. Self-Consistent Molecular Orbital Methods. XII. Further Extensions of Gaussian-Type Basis Sets for Use in Molecular Orbital Studies of Organic Molecules. *J. Chem. Phys.* **1972**, *56*, 2257−2261.

(52) Hariharan, P. C.; Pople, J. A. The Influence of Polarization Functions on Molecular Orbital Hydrogenation Energies. *Theor. Chim. Acta* **1973**, *28*, 213−222.

(53) Clark, T.; Chandrasekhar, J.; Spitznagel, G. W.; Schleyer, P. V. R. Efficient Diffuse Function-Augmented Basis Sets for Anion Calculations. III. The 3-21+G Basis Set for First-Row Elements, Li-F. *J. Comput. Chem.* **1983**, *4*, 294−301.

(54) Barone, V.; Uribe Grajales, L. M.; Di Grande, S.; Lazzari, F.; Mendolicchio, M. DFT Meets Wave-Function Methods for Accurate Structures and Rotational Constants of Histidine, Tryptophan, and Proline. *J. Phys. Chem. A* **2023**, *127*, 7534−7543.

(55) Barone, V. DFT Meets Wave-Function Composite Methods for Characterizing Cytosine Tautomers in the Gas Phase. *J. Chem. Theory Comput.* **2023**, *19*, 4970−4981.

(56) Caliebe, S. V.; Pinacho, P.; Schnell, M. Steroid Hormone Androsterone Observed in the Gas Phase by Rotational Spectroscopy. *J. Phys. Chem. Lett.* **2022**, *13*, 11913−11917.

(57) León, I.; Alonso, E. R.; Mata, S.; Alonso, J. L. Shape of testosterone. *J. Phys. Chem. Lett.* **2021**, *12*, 6983−6987.

(58) Pinacho, P.; Caliebe, S. V.; Quesada-Moreno, M. M.; Zinn, S.; Schnell, M. Unexpected Discovery of Estrone in the Rotational Spectrum of Estradiol: a Systematic Investigation of a CP-FTMW Spectrum. *Phys. Chem. Chem. Phys.* **2022**, *24*, 5539−5545.

(59) Zinn, S.; Schnell, M. Flexibility at the Fringes: Conformations of the Steroid Hormone β-Estradiol. *ChemPhysChem* **2018**, *19*, 2915−2920.

(60) Norman, A. W.; Henry, H. L. *Encyclopedia of Hormones*; Henry, H. L., Norman, A. W., Eds.; Academic Press: New York, 2003; pp 410−413.

(61) Chandramouli, B.; Del Galdo, S.; Fusè, M.; Barone, V.; Mancini, G. Two-Level Stochastic Search of Low-Energy Conformers For Molecular Spectroscopy: Implementation and Validation of MM and QM Models. *Phys. Chem. Chem. Phys.* **2019**, *21*, 19921−19934.

(62) Mancini, G.; Fusè, M.; Lazzari, F.; Chandramouli, B.; Barone, V. Unsupervised Search of Low-Lying Conformers With Spectroscopic Accuracy: a Two-Step Algorithm Rooted Into the Island Model Evolutionary Algorithm. *J. Chem. Phys.* **2020**, *153*, 124110.

(63) Kang, Y. K.; Park, H. S. Assessment of CCSD(T), MP2, DFT-D, CBS-QB3, and G4(MP2) Methods for Conformational Study of Alanine and Proline Dipeptides. *Chem. Phys. Lett.* **2014**, *600*, 112−117.

(64) Kesharwani, M. K.; Karton, A.; Martin, J. M. Benchmark ab Initio Conformational Energies for the Proteinogenic Amino Acids through Explicitly Correlated Methods. Assessment of Density Functional Methods. *J. Chem. Theory Comput.* **2016**, *12*, 444−454.

(65) Kang, Y. K.; Park, H. S. Exploring Conformational Preferences of Alanine Tetrapeptide by CCSD(T), MP2, and Dispersion- Corrected DFT Methods. *Chem. Phys. Lett.* **2018**, *702*, 69−75.

(66) Barone, V.; Fusè, M.; Lazzari, F.; Mancini, G. Benchmark Structures and Conformational Landscapes of Amino Acids in the Gas Phase: a Joint Venture of Machine Learning, Quantum Chemistry, and

Rotational Spectroscopy. *J. Chem. Theory Comput.* **2023**, *19*, 1243−1260.

(67) Barone, V.; Fusè, M. Accurate Structures and Spectroscopic Parameters of Phenylalanine and Tyrosine in the Gas-Phase: a Joint Venture of DFT and Composite Wave-Function Methods. *J. Phys. Chem. A* **2023**, *127*, 3648−3657.

(68) Barone, V. Accurate Structures and Spectroscopic Parameters of α, α-Dialkylated α-Amino Acids in the Gas-Phase: a Joint Venture of DFT and Wave-Function Composite Methods. *Phys. Chem. Chem. Phys.* **2023**, *25*, 22768−22774.

(69) Hait, D.; Head-Gordon, M. How Accurate is Density Functional Theory at Predicting Dipole Moments? An Assessment Using a New Database of 200 Benchmark Values. *J. Chem. Theory Comput.* **2018**, *14*, 1969−1981.

(70) Gordy, W.; Cook, R. L.; Weissberger, A. *Microwave Molecular Spectra*; Wiley: New York, 1984; Vol. *18*.

(71) Morishima, F.; Inokuchi, Y.; Ebata, T. Laser Spectroscopic Study of β-Estradiol and Its Monohydrated Clusters in a Supersonic Jet. *J. Phys. Chem. A* **2012**, *116*, 8201−8208.

(72) Ruoff, R. S.; Klots, T. D.; Emilsson, T.; Gutowsky, H. S. Relaxation of Conformers and Isomers in Seeded Supersonic Jets of Inert Gases. *J. Chem. Phys.* **1990**, *93*, 3142−3150.

(73) Godfrey, P. D.; Brown, R. D. Proportions of Species Observed in Jet Spectroscopy-Vibrational Energy Effects: Histamine Tautomers and Conformers. *J. Am. Chem. Soc.* **1998**, *120*, 10724−10732.

(74) Florio, G. M.; Christie, R. A.; Jordan, K. D.; Zwier, T. S. Conformational Preferences of Jet-Cooled Melatonin: Probing trans- and cis-Amide Regions of the Potential Energy Surface. *J. Am. Chem. Soc.* **2002**, *124*, 10236−10247.

(75) Knizia, G.; Adler, T. B.; Werner, H.-J. Simplified CCSD(T)-F12 methods: Theory and benchmarks. *J. Chem. Phys.* **2009**, *130*, 054104.

(76) Peterson, K. A.; Adler, T. B.; Werner, H.-J. Systematically Convergent Basis Sets for Explicitly Correlated Wavefunctions: The Atoms H, He, B−Ne, and Al−Ar. *J. Chem. Phys.* **2008**, *128*, 084102.

(77) Spackman, P. R.; Jayatilaka, D.; Karton, A. Basis Set Convergence of CCSD(T) Equilibrium Geometries Using a Large and Diverse Set of Molecular Structures. *J. Chem. Phys.* **2016**, *145*, 104101.

(78) Peterson, K. A.; Dunning, T. H. Accurate Correlation Consistent Basis Sets for Molecular Core−Valence Correlation Effects: The Second Row Atoms Al−Ar, and the First Row Atoms B−Ne Revisited. *J. Chem. Phys.* **2002**, *117*, 10548−10560.

(79) Margulès, L.; Demaison, J.; Rudolph, H. D. Ab-Initio and Experimental Structures of CH3NC. *J. Mol. Struct.* **2001**, *599*, 23−30.

(80) Dunning, T. H. Gaussian Basis Sets for Use in Correlated Molecular Calculations. I. The Atoms Boron Through Neon and Hydrogen. *J. Chem. Phys.* **1989**, *90*, 1007−1023.

(81) Cordero, B.; Gomez, V.; Platero-Prats, A. E.; Revés, M.; Echeverría, J.; Cremades, E.; Barragan, F.; Alvarez, S. Covalent Radii Revisited. *Dalton Trans.* **2008**, 2832−2838.

(82) Pauling, L. Atomic Radii and Interatomic Distances in Metals. *J. Am. Chem. Soc.* **1947**, *69*, 542−553.

(83) Barone, V.; Lazzari, F. Hunting for Complex Organic Molecules in the Interstellar Medium: the Role of Accurate Low-Cost Theoretical Geometries and Rotational Constants. *J. Phys. Chem. A* **2023**, *127*, 10517−10527.

(84) Frisch, M. J.; Trucks, G. W.; Schlegel, H. B.; Scuseria, G. E.; Robb, M. A.; Cheeseman, J. R.; Scalmani, G.; Barone, V.; Petersson, G. A.; Nakatsuji, H. *Gaussian 16*. Revision C.01; Gaussian Inc.: Wallingford CT, 2016.

(85) Vogt, N.; Vogt, J.; Demaison, J. Accuracy of the Rotational Constants. *J. Mol. Struct.* **2011**, *988*, 119−127.

(86) Barone, V. Quantum Chemistry Meets High-Resolution Spectroscopy for Characterizing the Molecular Bricks of Life in the Gas-Phase. *Phys. Chem. Chem. Phys.* **2024**, *26*, 5802−5821.

(87) Nielsen, H. H. The Vibration-Rotation Energies of Molecules. *Rev. Mod. Phys.* **1951**, *23*, 90−136.

(88) Schuurman, M. S.; Allen, W. D.; von Ragué Schleyer, P.; Schaefer, H. F. The Highly Anharmonic BH5 Potential Energy Surface Characterized in the Ab Initio Limit. *J. Chem. Phys.* **2005**, *122*, 104302.

(89) Yang, Q.; Mendolicchio, M.; Barone, V.; Bloino, J. Accuracy and Reliability in the Simulation of Vibrational Spectra: A Comprehensive Benchmark of Energies and Intensities Issuing from Generalized Vibrational Perturbation Theory to Second Order (GVPT2). *Frontiers Astron. Space Sci.* **2021**, *8*, 665232.

(90) Bloino, J.; Biczysko, M.; Barone, V. General Perturbative Approach for Spectroscopy, Thermodynamics, and Kinetics: Methodological Background and Benchmark Studies. *J. Chem. Theory Comput.* **2012**, *8*, 1015−1036.

(91) Yang, Q.; Bloino, J. An Effective and Automated Processing of Resonances in Vibrational Perturbation Theory Applied to Spectroscopy. *J. Phys. Chem. A* **2022**, *126*, 9276−9302.

(92) Martin, J. M.; Lee, T. J.; Taylor, P. R.; François, J. P. The Anharmonic Force Field of Ethylene, C2H4, by Means of Accurate Ab Initio Calculations. *J. Chem. Phys.* **1995**, *103*, 2589−2602.

(93) Krasnoshchekov, S.; Dobrolyubov, E.; Syzgantseva, M.; Palvelev, R. Rigorous Vibrational Fermi Resonance Criterion Revealed: Two Different Approaches Yield the Same Result. *Mol. Phys.* **2020**, *118*, No. e1743887.

(94) Mendolicchio, M.; Bloino, J.; Barone, V. General Perturb-Then-Diagonalize Model for the Vibrational Frequencies and Intensities of Molecules Belonging to Abelian and Non-Abelian Symmetry Groups. *J. Chem. Theory Comput.* **2021**, *17*, 4332−4358.

(95) Mendolicchio, M.; Bloino, J.; Barone, V. Perturb-Then-Diagonalize Vibrational Engine Exploiting Curvilinear Internal Coordinates. *J. Chem. Theory Comput.* **2022**, *18*, 7603−7619.

(96) Barone, V. Anharmonic Vibrational Properties by a Fully Automated Second Order Perturbative Approach. *J. Chem. Phys.* **2005**, *122*, 014108.

(97) Franke, P. R.; Stanton, J. F.; Douberly, G. E. How to VPT2: Accurate and Intuitive Simulations of CH Stretching Infrared Spectra Using VPT2+K with Large Effective Hamiltonian Resonance Treatments. *J. Phys. Chem. A* **2021**, *125*, 1301−1324.

(98) Irikura, K. K.; Johnson, R.; Kacker, R. N.; Kessel, R. Uncertainties in Scaling Factors for Ab Initio Vibrational Zero Point Energies. *J. Chem. Phys.* **2009**, *130*, 114102.

(99) Kesharwani, M. K.; Brauer, B.; Martin, J. M. L. Frequency and Zero-Point Vibrational Energy Scale Factors for Double-Hybrid Density Functionals (and Other Selected Methods): Can Anharmonic Force Fields Be Avoided? *J. Phys. Chem. A* **2015**, *119*, 1701−1714.

(100) Chan, B.; Radom, L. Frequency Scale Factors for Some Double-Hybrid Density Functional Theory Procedures: Accurate Thermochemical Components for High-Level Composite Protocols. *J. Chem. Theory Comput.* **2016**, *12*, 3774−3780.

(101) Zapata Trujillo, J. C.; McKemmish, L. K. Model Chemistry Recommendations for Scaled Harmonic Frequency Calculations: A Benchmark Study. *J. Phys. Chem. A* **2023**, *127*, 1715−1735.

(102) Lin, C. Y.; Gilbert, A. T. B.; Gill, P. M. W. Calculating Molecular Vibrational Spectra Beyond the Harmonic Approximation. *Theor. Chem. Acc.* **2008**, *120*, 23−35.

(103) Juanes, M.; Li, W.; Spada, L.; Evangelisti, L.; Lesarri, A.; Caminati, W. Internal Dynamics of Cyclohexanol and the Cyclohexanol−Water Adduct. *Phys. Chem. Chem. Phys.* **2019**, *21*, 3676−3682.

(104) Kolesnikova, L.; Daly, A. M.; Alonso, J. L.; Tercero, B.; Cernicharo, J. The Millimeter Wave Tunneling−Rotational Spectrum of Phenol. *J. Mol. Spectrosc.* **2013**, *289*, 13−20.

(105) Demaison, J.; Craig, N. C.; Groner, P.; Ecija, P.; Cocinero, E. J.; Lesarri, A.; Rudolph, H. D. Accurate Equilibrium Structures for Piperidine and Cyclohexane. *J. Phys. Chem. A* **2015**, *119*, 1486−1493.

(106) Kim, H.; Gwinn, W. Ring Puckering in Five-Membered Rings. III. The Microwave Spectrum, Dipole Moment, and Structure of Cyclopentanone. *J. Chem. Phys.* **1969**, *51*, 1815−1819.

(107) Wachsmuth, D.; Jahn, M. K.; Blanco, S.; Gigosos, M. A.; Lesarri, A.; Grabow, J.-U. Inversion of Bicyclic Decanes: Rotational Spectra of the Trans and Double Cis Conformations of 2-Decalone. *ChemPhysChem* **2017**, *18*, 3620−3624.

(108) Brown, G. G.; Dian, B. C.; Douglass, K. O.; Geyer, S. M.; Shipman, S. T.; Pate, B. H. A broadband Fourier Transform Microwave

Spectrometer Based on Chirped Pulse Excitation. *Rev. Sci. Instrum.* **2008**, *79*, 1−13.

(109) Cosentino, U.; Villa, A.; Pitea, D.; Moro, G.; Barone, V.; Maiocchi, A. Conformational Characterization of Lanthanide(III)-DOTA Complexes by Ab Initio Investigation in Vacuo and in Aqueous Solution. *J. Am. Chem. Soc.* **2002**, *124*, 4901−4909.